ADVANCED MATERIALS
www.advmat.de

High-Voltage Lithium-Metal Batteries Enabled by Localized High-Concentration Electrolytes

*Shuru Chen, Jianming Zheng, Donghai Mei, Kee Sung Han, Mark H. Engelhard, Wengao Zhao, Wu Xu, Jun Liu, and Ji-Guang Zhang**

Rechargeable lithium-metal batteries (LMBs) are regarded as the "holy grail" of energy-storage systems, but the electrolytes that are highly stable with both a lithium-metal anode and high-voltage cathodes still remain a great challenge. Here a novel "localized high-concentration electrolyte" (HCE; 1.2 M lithium bis(fluorosulfonyl)imide in a mixture of dimethyl carbonate/bis(2,2,2-trifluoroethyl) ether (1:2 by mol)) is reported that enables dendrite-free cycling of lithium-metal anodes with high Coulombic efficiency (99.5%) and excellent capacity retention (>80% after 700 cycles) of Li||$LiNi_{1/3}Mn_{1/3}Co_{1/3}O_2$ batteries. Unlike the HCEs reported before, the electrolyte reported in this work exhibits low concentration, low cost, low viscosity, improved conductivity, and good wettability that make LMBs closer to practical applications. The fundamental concept of "localized HCEs" developed in this work can also be applied to other battery systems, sensors, supercapacitors, and other electrochemical systems.

With the eventual maturation of the state-of-the-art lithium (Li)-ion batteries (LIBs),[1] rechargeable Li-metal batteries (LMBs) have been regarded as the "holy grail" for the next generation of high-energy storage systems.[2] However, they typically exhibit very poor performance and safety concern due to early failure of Li-metal anodes (LMAs) induced by instability of Li|electrolyte interface and dendrite growth during repeated Li plating/stripping.[3] Among various factors that affect the performance of an LMB, the electrolyte thus plays a dominant role.[4] Commercial electrolytes used in LIBs (typically 1–1.2 M lithium hexafluorophosphate ($LiPF_6$) in a mixture of carbonate solvents) are not suitable for LMBs because they will lead to dendritic growth and very low Coulombic efficiency (CE) of LMAs.[5] In recent years, high-concentration electrolytes (HCEs, e.g., >3 M) have received much attention because their unusual functionalities effectively improve the interfacial stability between electrode and electrolyte in various battery systems.[6] For example, we reported an ether-based HCE (i.e., 4 M lithium bis(fluorosulfonyl) imide (LiFSI) in 1,2-dimethoxyethane (DME)) that can improve the CE of LMAs to 99.2%, but this HCE is not compatible with 4 V-class cathodes.[6h,i] By replacing DME with dimethyl carbonate (DMC), Yamada et al. demonstrated that an HCE consisting of 5.5 M LiFSI in DMC can be stable with 5 V-class cathodes, but its stability with LMAs remains in question.[6j] In addition, HCEs also exhibit high cost (which is proportional to the salt concentration), poor ionic conductivity, and poor wetting capability, which hindered their practical applications. In recent years, several groups have used a cosolvent with an HCE to overcome these disadvantages.[7] For exmaple, Watanabe and coworkers used hydrofluoroether (HFE), 1,1,2,2-tetrafluoroethyl 2,2,3,3-tetrafluoropropyl ether to dilute solvate ionic liquid electrolytes (concentrated bis(trifluoromethanesulfonyl)imide (LiTFSI or LiTFSA) in glymes) and suppress the dissolution of Li_2S_m in the Li–S batteries. They indicate that the addition of HFE does not break the solvate structure of the glyme–Li salt molten complexes and greatly enhances the power density of the Li–S batteries.[7d] They also diluted solvate ionic liquids (SILs) with selected molecular solvents and determined the stability of the complex cations in the diluted SILs.[7e] In a separate work, Doi et al. used a fluorinated ether diluted concentrated $LiBF_4$ in propylene carbonate for 4 V-class LMBs.[7f] However, the CE of LMAs in this electrolyte is found to be less than 60% (Figure S1, Supporting Information) which is not suitable for rechargeable LMBs. In fact, none of the diluted HCEs reported to date are highly stable with both LMAs and high-voltage cathodes at the same time. Therefore, the design of electrolytes that are compatible with both LMAs and high-voltage cathodes (e.g., $LiNi_xMn_yCo_zO_2$) is very critical for high-energy rechargeable LMBs, which still remains a great challenge.

In this work, we report localized high-concentration electrolytes (LHCEs) by diluting an HCE with an "inert" diluent, meaning that the diluent itself exhibits similar or even wider electrochemical stability window compared to the HCE, which also does not dissolve the salt but is miscible with the solvent and the Li^+-solvent solvates in the HCE. Therefore it does not

Dr. S. Chen, Dr. J. Zheng, W. Zhao, Dr. W. Xu, Dr. J. Liu, Dr. J.-G. Zhang
Energy and Environment Directorate
Pacific Northwest National Laboratory
902 Battelle Boulevard, Richland, WA 99352, USA
E-mail: Jiguang.zhang@pnnl.gov
Dr. D. Mei, Dr. K. S. Han, Dr. M. H. Engelhard
Physical and Computational Sciences Directorate
Pacific Northwest National Laboratory
902 Battelle Boulevard, Richland, WA 99352, USA
The ORCID identification number(s) for the author(s) of this article can be found under https://doi.org/10.1002/adma.201706102.

DOI: 10.1002/adma.201706102

affect the original Li salt-solvent coordination in the HCE, but it does significantly lower the total Li salt concentration to a more practical level while preserving (or even enhancing) the unique characteristics of the HCE. LHCE can be regarded as an HCE mixed with diluent in molecular level. Although both HCE and diluent contact LMA, Li^+ ions will preferentially move within the localized HCE region. Based on this principle, by careful selections of lithium salts, solvents, and diluents, we developed LHCEs that are stable with both Li-metal and 4 V-class cathodes, and demonstrate dendrite-free cycling of LMAs with high CE in Li||Cu cells and excellent cycling stability of Li||$LiNi_{1/3}Mn_{1/3}Co_{1/3}O_2$ batteries.

A typical example of the LHCEs developed in this work consists of an HCE (i.e., 5.5 M LiFSI/DMC) diluted by bis(2,2,2-trifluoroethyl) ether (BTFE) to form LHCEs with saturated LiFSI concentration ranging from 3.8 to 1.2 M (corresponding to DMC/BTFE molar ratios of 1:0.5, 1:1, 1:1.5, and 1:2 (Table S1, Supporting Information). The CEs of LMAs in these electrolytes were first investigated in Li||Cu cells using a ten cycle average approach combined with a conditional procedure (See Methods in the Supporting Information) at a current density of 0.5 mA cm^{-2}.[8] The results are shown in **Figure 1** and Figure S2 (Supporting Information). In the 1.2 M LiFSI/DMC electrolyte, the CE of the LMA is very low (<10%, Figure 1a). Similar low CE (<50%, Figure S2a, Supporting Information) was also observed using a conventional electrolyte of 1.0 M $LiPF_6$/ethylene carbonate (EC)–ethyl methyl carbonate (EMC) (4:6 by wt%). In contrast, the CE of the LMA increases to as high as 99.2% when cycled in HCEs consisting of 3.7–5.5 M LiFSI/DMC (Figure 1b; Figure S2b, Supporting Information). More importantly, LMAs cycled in all the LHCEs with reduced LiFSI concentration of 3.8–1.2 M, prepared by diluting the HCEs with various contents of BTFE, have demonstrated improved CEs from 99.3% to 99.5% (Figure 1c,d; Figure S2c,d, Supporting Information). The effects of current density on CE of LMAs were also studied using the LHCE of 1.2 M LiFSI/DMC-BTFE (1:2 by mol) (Figure S3, Supporting Information). A high CE of 99.4% and 98.9% was still achieved at a higher current density of 1.0 and 3.0 mA cm^{-2}, respectively, despite of a much lower CE of 92.6% when current density was further increased to 5.0 mA cm^{-2}. The current density of 3.0 mA cm^{-2} is equivalent to 1 C rate for cells with practical areal capacity loading of 3.0 mAh cm^{-2}, which is high enough for most applications. A linear increase in the average potential for Li stripping was also noticed; however, the overpotential is only ≈120 mV even at a very high current density of 5.0 mA cm^{-2}, suggesting good reaction kinetics in the LHCE.

In addition to the high CE, long-term cycling stability of LMAs is also critical for rechargeable LMBs. The evolution of voltage profiles and CEs of Li||Cu cells during Li plating/stripping were further examined at a current density of 0.5 mA cm^{-2} with areal capacity of 1 mAh cm^{-2} (Figure S4, Supporting Information). Despite the high CE of ≈99% measured by the ten cycle average method, the HCE of 3.7 M LiFSI/DMC can only enable ≈100 stable cycles under repeated Li plating/stripping, followed by a dramatic increase in cell polarization and fast drop in the CEs. In contrast, cells with both the HCE of 5.5 M LiFSI/DMC and the LHCE of 1.2 M LiFSI/DMC-BTFE (1:2 by mol)

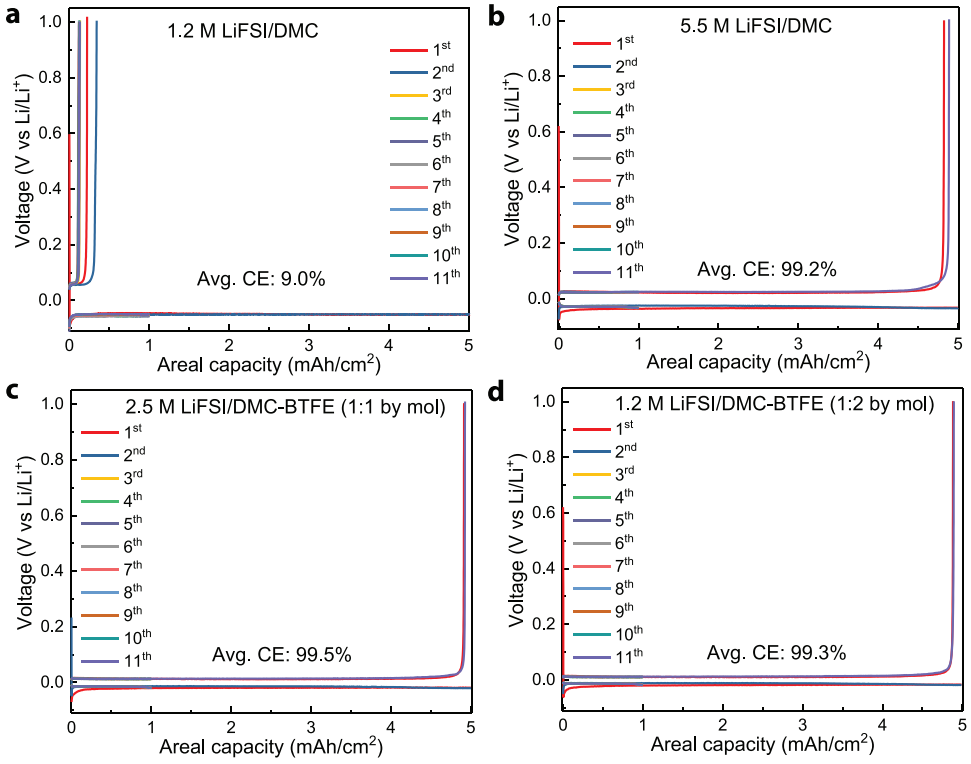

Figure 1. Coulombic efficiency of Li-metal plating/stripping using Li||Cu cells in different electrolytes. a) Dilute 1.2 M LiFSI/DMC; b) highly concentrated 5.5 M LiFSI/DMC; c) moderately diluted 2.5 M LiFSI/DMC-BTFE (1:1 by mol), and d) highly diluted 1.2 M LiFSI/DMC-BTFE (1:2 by mol). The current density is 0.5 mA cm^{-2}.

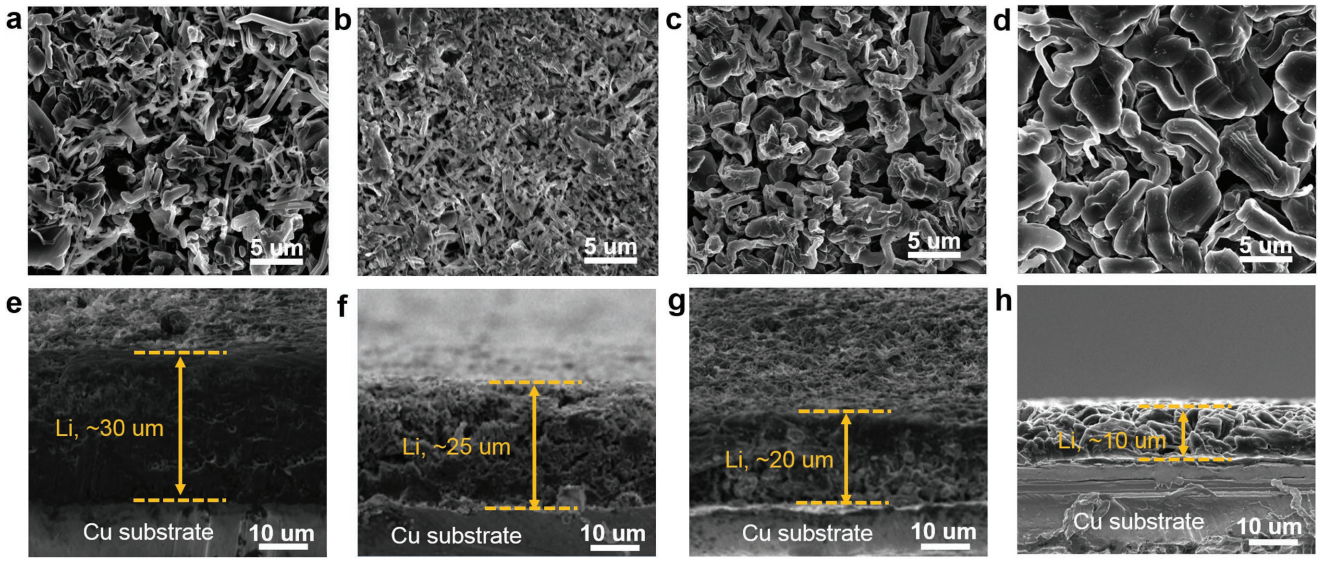

Figure 2. a–d) Top and e–h) cross-sectional views of SEM images in the conventional 1.0 M $LiPF_6$/EC-EMC (4:6 by wt%) (a,e), dilute 1.2 M LiFSI/DMC (b,f), the HCE of 5.5 M LiFSI/DMC (c,g), and the LHCE of 1.2 M LiFSI/DMC-BTFE (1:2 by mol) (d,h). SEM images of Li deposits were obtained by plating 1.5 mAh cm^{-2} Li on Cu substrate at a current density of 1.0 mA cm^{-2}.

are stable for more than 200 cycles, with an average CE of ≈99% and without obvious voltage polarization increase. However, the electrode polarisation during cycling in the LHCE is much lower than that in the HCEs, and this difference becomes more obvious in Li‖Li symmetric cells with increasing current densities (Figure S5, Supporting Information) due to the reduced viscosity and improved ionic conductivity of the LHCE (Table S1, Supporting Information).

Striking differences in morphologies of Li deposits in different electrolytes were observed by scanning electron microscopy (SEM) images (**Figure 2**). Highly porous/loose structures with extensive dendritic Li growth were observed in both conventional electrolyte and dilute 1.2 M LiFSI/DMC (this is consistent with their low CEs). The most striking difference was observed when the LHCE of 1.2 M LiFSI/DMC-BTFE (1:2 by mol) was used, where compact aggregates of large nodule-like Li particles (≈5 µm) without dendrites were formed. Moreover, with increasing current densities (2, 5, and 10 mA cm^{-2}), the Li deposits remained nodule-like in the LHCE even though the particle sizes decreased slightly with increasing current densities (Figure S6, Supporting Information). It is also worth noting that the thickness of the Li film deposited in the conventional electrolyte (≈30 µm), dilute 1.2 M LiFSI/DMC (≈25 µm), and the HCE (≈20 µm) is much higher than the theoretical thickness of Li (≈7.2 µm for a capacity of 1.5 mAh cm^{-2}). In contrast, the thickness of the Li film deposited in the LHCE is only ≈10 µm, which is much closer to the theoretical value. This value represents one of the most compact Li films obtained by electrochemical deposition. Formation of high density, low surface area nodule-like Li deposits of large particle size can greatly mitigate the interfacial reactions with electrolytes, and thus lead to high CE, improved cycle life, and better safety of LMAs.

Recently, Yamada and co-workers showed that highly concentrated LiFSI/DMC electrolytes can suppress Al corrosion even at >5 V, while continuous Al dissolution was found in dilute LiFSI/DMC electrolytes at 4.3 V, which led to unlimited overcharging.[6j] The anodic corrosion of an aluminum (Al) current collector in BTFE diluted LHCEs is also examined to insure its high-voltage stability by linear scan voltammetry (LSV) on Li‖Al cells. As shown in Figure S7 in the Supporting Information, despite decreasing anodic stability with increasing content of BTFE diluent, Al corrosion can be still suppressed even with the most diluted 1.2 M LiFSI/DMC-BTFE (1:2 by mol) at >4.5 V. This window should be sufficient for most commercial 4-V class cathodes. $LiNi_{1/3}Mn_{1/3}Co_{1/3}O_2$ (NMC) with an areal capacity of 2.0 mAh cm^{-2} was then used as a baseline cathode to investigate the stability of LMBs in the LHCE of 1.2 M LiFSI/DMC-BTFE (1:2 by mol). Li‖NMC cells with the HCE (5.5 M LiFSI/DMC) and conventional electrolyte (1.0 M $LiPF_6$/EC-EMC (4:6 by wt%)) were also investigated for comparison (**Figure 3**). As shown in Figure 3a, during the first three formation cycles at 0.2 mA cm^{-2} (C/10 rate), the Li‖NMC cells delivered similar specific discharge capacities of ≈160 mAh g^{-1} (based on the weight of NMC) after charging to 4.3 V. In the following cycles at a high charge/discharge current density of 2.0 mA cm^{-2} (1 C rate), the Li‖NMC cell with conventional electrolyte showed a drastic increase of electrode polarization (Figure S8a, Supporting Information) and fast capacity degradation (only 40% retention after 100 cycles) with low cycling efficiency (avg. < 98%), most probably due to severe corrosion of the LMA.[2j] In the HCE, despite its improved CE and the high-voltage stability, the Li‖NMC cell shows a low discharge capacity of ≈140 mAh g^{-1} with continuous fading and obvious increase of electrode polarization (Figure S8b, Supporting Information), retaining only 76% of its capacity after 100 cycles. This can be attributed to sluggish electrode reaction kinetics at high current density resulting from the high viscosity, low conductivity, and poor wetting ability of the HCE. In sharp contrast, the Li‖NMC cell with the LHCE demonstrated high discharge capacity of ≈150 mAh g^{-1} and excellent

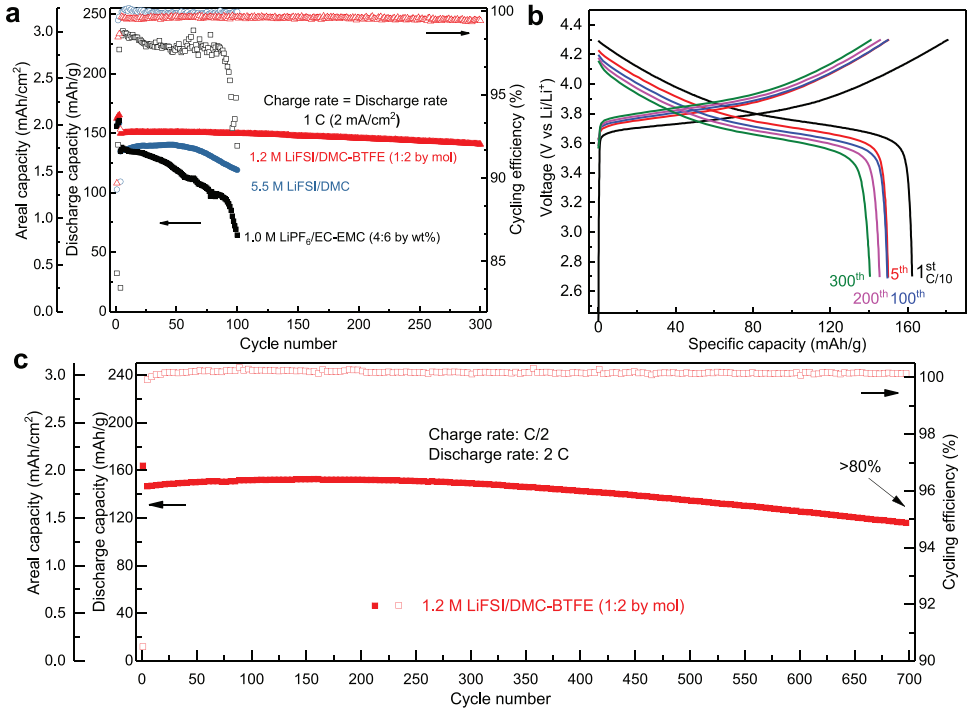

Figure 3. a) Cycling stability and efficiency with different electrolytes at the charge/discharge rate of 2 mA cm^{-2} (1 C) after three formation cycles at 0.2 mA cm^{-2} (C/10) in the voltage range of 2.7–4.3 V at 30 °C. b) Evolution of voltage profiles upon cycling in 1.2 M LiFSI/DMC-BTFE (1:2 by mol). c) Cycling stability and efficiency with 1.2 M LiFSI/DMC-BTFE (1:2 by mol) at C/2 charge and 2 C discharge rates.

long-term cycling stability (≈95% after 300 cycles), with an average cycling efficiency of ≈99.7% and limited increase of electrode polarisation (Figure 3b). Moreover, when cycled at a slower charge rate of C/2 and a faster discharge rate of 2 C, the cell with the LHCE can deliver a similar high discharge capacity of ≈150 mAh g^{-1} and retain >80% capacity even after 700 cycles (Figure 3c).

Rate performance of Li||NMC batteries has also been investigated using two charge/discharge protocols: (i) charge at the same rate (C/5) and discharge at different rates; (ii) charge at different rates and discharge at the same rate (C/5). As shown in Figure S9 in the Supporting Information, Li||NMC batteries using the LHCE exhibit superior charging and discharging capabilities as compared to those with the HCE and the conventional electrolyte. In particular, with protocol (i), when discharging at 5C (i.e., 10 mA cm^{-2}), the battery using LHCE is still able to deliver a high discharge capacity of 141 mAh g^{-1}, which is much higher than the 116 and 68 mAh g^{-1} for the batteries using HCE and conventional electrolyte, respectively. The greatly enhanced rate capability using LHCE compared to that using HCE could be attributed to the improved interfacial reaction kinetics (Figure S10, Supporting Information) resulting from the reduced viscosity, increased conductivity, and improved electrode/separator wetting.

The exceptional electrochemical performance of LMBs achieved with the LHCEs is directly related to their localized highly concentrated solvation structures and the selective reductive properties of electrolyte components over the Li-metal surface, which ensures their cycling stability toward both the LMA and the NMC cathode. Density functional theory (DFT) calculation shows that the interaction between LiFSI and BTFE (–41.4 kJ mol^{-1}) is much weaker than that between LiFSI and the DMC solvent (–88.7 kJ mol^{-1}). Therefore, LiFSI is preferentially coordinated with DMC, independent of the content of BTFE diluent, as shown by the radial distribution functions of Li–O_{DMC} and Li–O_{BTFE} pairs (**Figure 4**a) calculated from ab initio molecular dynamics (AIMD) simulation trajectories (Figure S11, Supporting Information). A sharp peak of the Li–O_{DMC} pair is identified at 1.95 Å for all three studied systems, while two small peaks of the Li–O_{BTFE} pair at 4.65 and 5.63 Å are found for two ternary solution systems with high and low BTFE contents, respectively. This strongly suggests that the Li$^+$ cation solvation occurs mainly by DMC molecules, while BTFE interaction with other electrolyte components is very weak, which clearly indicates the existence of the localized highly concentrated LiFSI–DMC pairs.

To confirm this, we further investigated the progression of Raman spectra for electrolytes with different salt concentrations in pure DMC and DMC/BTFE mixtures (Figure 4b). With increasing LiFSI salt concentration up to 5.5 M in pure DMC, the free DMC (O–CH_3 stretching vibration band at ≈920 cm^{-1}) gradually diminishes to form Li$^+$-coordinated DMC (≈940 cm^{-1}). With dilution of BTFE, the Li$^+$-coordinated DMC solvation structure is well preserved and the vibration band of BTFE at 830–840 cm^{-1} does not change in different LiFSI/DMC-BTFE solutions. Notably, the dilution with BTFE slightly weakens the association between Li$^+$ cations and FSI$^-$ anions, as evidenced by the downshift of the FSI$^-$ Raman band (710–780 cm^{-1}); this would be beneficial for enhancing the Li$^+$

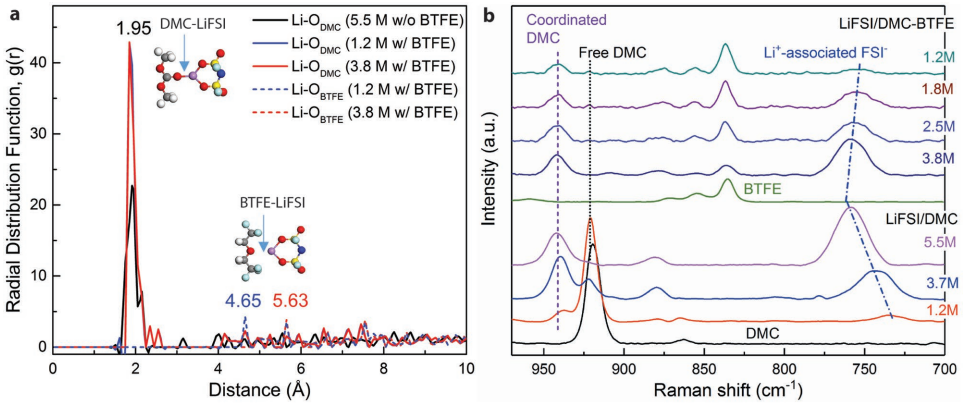

Figure 4. a) Radial distribution functions of Li–O_{DMC} and Li–O_{BTFE} pairs calculated from AIMD simulation trajectories at 30 °C, with insets showing the structures of DMC–LiFSI and BTFE–LiFSI solvent-salt pairs. b) Progression of Raman spectra with different salt concentrations in pure DMC and various DMC/BTFE mixtures.

ion diffusion, and for improving the ionic conductivity and kinetic properties of the electrolytes.

The LHCE solvation structure was also confirmed by pulsed field gradient-nuclear magnetic resonance (PFG-NMR) results as shown in Figure S12 in the Supporting Information. All diffusion coefficients (*D*s) of electrolyte components are globally proportional to the inverse of viscosity (η^{-1}) of solutions, while their variations are slightly different depending on the local ion–ion and ion–solvent interactions as predicted by the Stokes–Einstein theory of diffusion.[9] It was found that $D_{DMC} > D_{BTFE}$ in pure DMC, BTFE solvent, and their mixture, but with introduction of LiFSI salt, D_{DMC} and D_{BTFE} become smaller and larger compared to η^{-1}, respectively. This strongly suggests that the Li^+ cation solvation occurs mainly by DMC molecules, while BTFE interaction with other electrolyte components is quite weak. It also indicates that Li^+ cation diffusion is enhanced ($D_{Li} \geq D_{FSI}$) by addition of BTFE, which is consistent with Raman observations, while the reverse is the case in the LiFSI/DMC electrolytes ($D_{Li} \leq D_{FSI}$). The stable diffusion ratios D_{Li}/D_{DMC} and D_{FSI}/D_{DMC} suggest that the LHCE solvation structure composed of Li^+ cation, FSI^- anion, and DMC solvent is not sensitive to the population of BTFE in the LiFSI/DMC-BTFE electrolytes.

To investigate the interaction between the LMA and electrolytes, Bader charge analysis was used to obtain the possible charge transfer between the electrolyte solvents and the salt species upon adsorption on the most stable Li (100) surface (Figure S13, Supporting Information). The interaction between BTFE and the Li anode surface is very weak compared with those of DMC, LiFSI, and the DMC–LiFSI pair, indicating that the BTFE molecule is relatively almost inert and barely being reduced. DMC and the DMC–LiFSI pair can be slightly reduced by obtaining the fractional charges of –0.19 and –0.40 |e|, respectively, implying that both are reduced preferentially, thus leading to possible decomposition (Table S2, Supporting Information). The reductive stability of absorbed electrolyte components was further investigated using the lowest unoccupied molecular orbital (LUMO) energies. The electrolyte component with the lowest LUMO energy is the component that will be reduced first to form a solid electrolyte interphase (SEI) layer during the cycling process. Figure S14 in the Supporting Information shows that LUMOs of the conduction bands, which are located on DMC in 1.2 M LiFSI/DMC, are shifted to FSI^- in both the HCE and LHCE. Therefore, FSI^- anions rather than DMC solvents will decompose first as the dominant reduction reaction,[6c] forming a robust FSI-derived SEI layer (rich in LiF and/or Li_2O according to X-ray photoelectron spectroscopy (XPS) results in **Figure 5**c and Figure S15 and Table S3 (Supporting Information)). Unlike the SEI layers formed in the conventional electrolyte (Figure 5a), the FSI-derived SEI layers in the LHCE exhibit a distinctive feature (Figure 5b) consisting of porous interconnected films a few nanometers thick after the nodule-like Li deposits were completely removed. This FSI-derived SEI layer is free of isolated "dead" Li blocks, indicating that it serves as a good electron barrier preventing the further reduction of electrolyte while facilitating Li^+ migration, and thus leads to high CE, good stability, and enhanced safety of LMAs for LMBs.

In summary, we have developed an LHCE that enables dendrite-free Li cycling with a high CE (up to 99.5%) and greatly enhanced cycling stability of Li||NMC batteries. The fundamental concept of LHCE can also be applied to lithium-metal batteries using other electrolytes (such as carbonate-based (Figure S16, Supporting Information) and ether-based electrolytes (Figure S17, Supporting Information)), Li–S batteries, Li–air batteries, sodium metal batteries, and aqueous-based lithium ion batteries. Therefore, it opens a new avenue for the development of multifunctional electrolytes for broad application.

Experimental Section

Materials Preparation: $LiPF_6$, DMC, EC, EMC (all in battery-grade purity), and $LiNi_{1/3}Mn_{1/3}Co_{1/3}O_2$ were obtained from BASF Corporation. LiFSI (Nippon Shokubai) was used after drying at 120 °C in vacuum for 24 h. BTFE (99%) from SynQuest Labs was dried with molecular sieves prior to use. The electrolytes were prepared by dissolving the desired amount of salt into the solvent mixtures in an Ar-filled glovebox. Li chips (450 µm, area 1.91 cm^2) were purchased from MTI Corporation. The cathode was prepared by mixing NMC, Super C carbon, and polyvinylidene fluoride binder at a mass ratio of 96:2:2 in *N*-methyl-2-pyrrolidone and coating the slurry onto Al foil. The electrode laminates

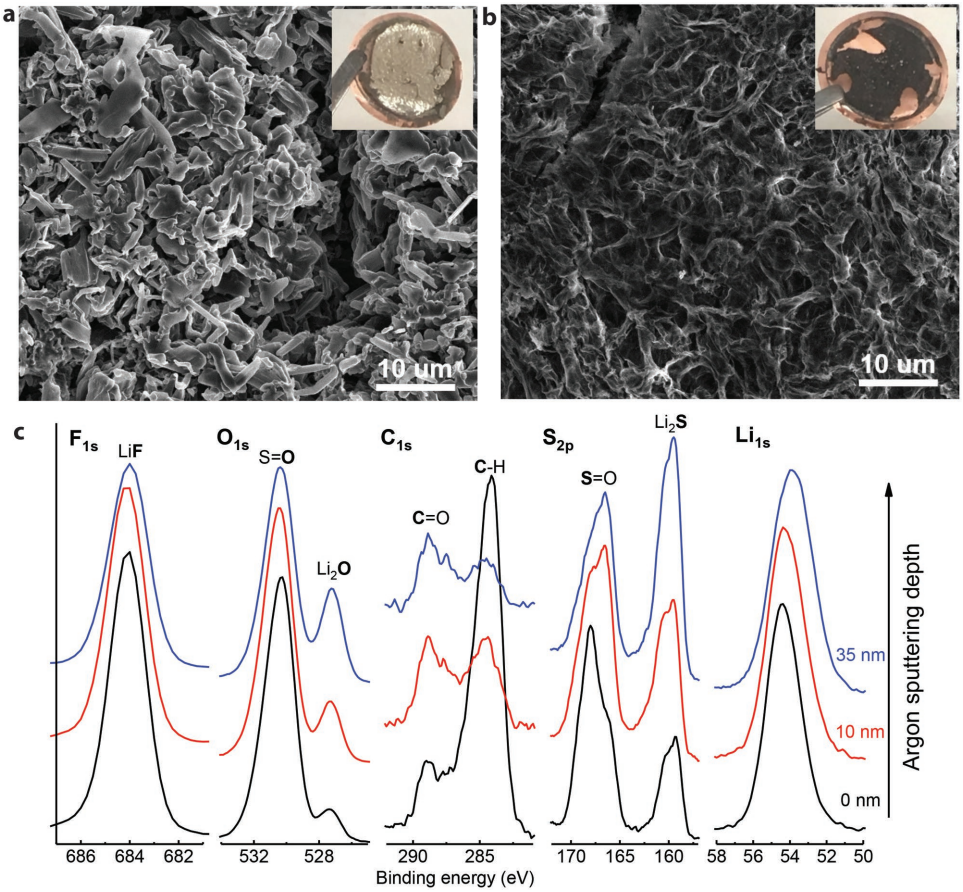

Figure 5. a,b) SEM images of the SEI on Cu electrodes in conventional electrolyte of: (a) 1.0 M $LiPF_6$/EC-EMC (4:6 by wt%) and the LHCE of (b) 1.2 M LiFSI/DMC-BTFE (1:2 by mol). Insets are optical photos of the cycled Cu electrodes. The working area of the Cu substrate is 2.11 cm^2. c) XPS spectral regions for F 1s, O 1s, C 1s, S 2p, and Li 1s at various argon (Ar^+) sputtering depths on the SEI accumulated on Cu substrate and collected by disassembling Li||Cu cells after ten cycles at a current density of 1 mA cm^{-2} with a capacity of 5 mAh cm^{-2}.

were punched into discs (1.27 cm^2) after drying at ≈75 °C under vacuum for 12 h.

Materials Characterizations: Raman spectra were collected using a Horiba LabRAM HR Raman spectrometer with spectral resolution of 1 cm^{-1}, with electrolytes sealed in a glass tube. The viscosity (η) of the electrolytes was measured on a Brookfield DV-II+ Pro viscometer at 30 °C. The ionic conductivity of electrolytes was measured using a BioLogic MCS 10 fully integrated multichannel conductivity spectrometer with cells made of two parallel Pt electrodes at 30 °C. The conductivity cell constants were predetermined using conductivity standard solution from Oakton Inc. Morphology observations were performed on an FEI Quanta or Helios focused ion beam SEM at 5.0 kV. The cross sections were obtained by cutting the electrodes with a razor blade. For SEM and XPS, the cycled electrodes were soaked in pure DMC for 10 min and then rinsed with pure DMC at least three times to eliminate remaining electrolytes, and finally dried under vacuum. They were transported from the glovebox to the SEM and XPS instruments in a hermetically sealed container protected by Ar gas. The experimental details for XPS and NMR measurements are shown in Methods in the Supporting Information.

Electrochemical Measurements: Electrochemical cycling tests were carried out using CR2032-type coin cells on Land BT2000 and Arbin BT-2000 battery testers at 30 °C in environmental chambers. Li||Cu, Li||Al, Li||Li, and Li||NMC cells were assembled in the glove box with a Li chip as both the counter and reference electrodes. Celgard 2500 (polypropylene, pp) was used as the separators except for cells with 5.5 M LiFSI/DMC electrolyte, where Celgard 3501 (surfactant-coated pp) was used to ensure good wetting due to a wettability issue with Celgard 2500. To standardize the testing, 200 µL of electrolyte was added to each coin cell even though some would spill out during cell crimping.

For Li||Cu cells, the effective area of the Cu foil disc (diameter 1.90 cm) for Li deposition was 2.11 cm^2 (diameter 1.64 cm). During each cycle, a designated amount of Li was deposited on the Cu substrate at a specific current density and then stripped until the potential reached 1.0 V versus Li/Li^+. All the Li||NMC batteries were assembled using Al-clad coin cell cans covered with an additional Al foil disc (diameter 1.90 cm) for the cathode part to avoid the corrosion of a stainless steel can and the side effects at high voltage, and tested between 2.7 and 4.3 V. 1 C is equal to 160 mA g^{-1} (which is ≈2 mA cm^{-2}) of active NMC materials.

LSV studies of the electrolyte solutions were conducted in Li||Al coin cells using an Al foil disc (diameter 1.90 cm, effective area 2.11 cm^2) as working electrode on a CHI660C workstation with a scan rate of 0.2 mV s^{-1} from open-circuit voltage to 6 V.

CE Measurement: The following protocol was used to measure average CE of the LMA accurately using a Li||Cu coin cell: (1) Perform one initial formation cycle with Li plating of 5 mAh cm^{-2} on Cu and stripping to 1 V; (2) Plate 5 mAh cm^{-2} Li on Cu as Li reservoir; (3) Repeatedly strip/plate Li with 1 mAh cm^{-2} (or strip to 1 V if overpotential > 1 V is needed to strip Li with 1 mAh cm^{-2}) for nine cycles; (4) Strip all Li to 1 V. Current: 0.5 mA cm^{-2}. Avg. CE is calculated by dividing the total stripping capacity by the total plating capacity after the formation cycle based on Equation (1):

$$CE_{avg.} = \frac{nQ_{cycle,strip} + Q_{strip}}{nQ_{cycle,plate} + Q_{reservoir}} \times 100 \quad (1)$$

where n is the cycle number at the charge capacity of $Q_{cycle,strip}$ and discharge capacity of $Q_{cycle,plate}$,Q_{strip} is the charge capacity during the final stripping, and $Q_{reservoir}$ is the discharge capacity during step (2).

MD Simulations: First-principles DFT and AIMD simulations were used to characterise the LiFSI–DMC solvation structure in the electrolytes. All calculations were performed using the Vienna ab initio simulation package.[10] More details are shown in the Supporting Information.

Supporting Information

Supporting Information is available from the Wiley Online Library or from the author.

Acknowledgements

S.C. and J.Z. contributed equally to this work. This work was supported by the Assistant Secretary for Energy Efficiency and Renewable Energy, Office of Vehicle Technologies of the U.S. Department of Energy (DOE) through the Advanced Battery Materials Research (BMR) program and the Battery500 Consortium under contract no. DE-AC02-05CH11231. The microscopy and spectroscopy measurements were performed using the Environmental Molecular Sciences Laboratory, a DOE Office of Science User Facility sponsored by the Office of Biological and Environmental Research. Pacific Northwest National Laboratory is operated by Battelle for the DOE under Contract DE-AC05-76RL01830. The authors would like to thank Qiuyan Li for preparing the NMC cathode electrodes and Patrick Z. El Khoury for helping with Raman characterisation.

Conflict of Interest

The authors declare no conflict of interest.

Keywords

anode, batteries, high voltage, lithium, localized high-concentration electrolyte

Received: October 19, 2017
Revised: January 18, 2018
Published online: March 25, 2018

[1] a) J. M. Tarascon, M. Armand, *Nature* **2001**, *414*, 359; b) J. B. Goodenough, K.-S. Park, *J. Am. Chem. Soc.* **2013**, *135*, 1167; c) M. S. Whittingham, *Proc. IEEE* **2012**, *100*, 1518.

[2] a) D. Aurbach, Y. Cohen, *J. Electrochem. Soc.* **1996**, *143*, 3525; b) M. B. Armand, P. G. Bruce, M. Forsyth, B. Scrosati, W. Wieczorek, *in Energy Materials*, (Eds: D. W. Bruce, D. O'Hare, R. I. Walton), John Wiley & Sons Ltd, Chichester, UK **2011**, https://doi.org/10.1002/9780470977798.ch1; c) Y. Lu, Z. Tu, L. A. Archer, *Nat. Mater.* **2014**, *13*, 961; d) D. Lin, Y. Liu, Y. Cui, *Nat. Nanotechnol.* **2017**, *12*, 194; e) J.-G. Zhang, W. Xu, W. A. Henderson, *Lithium Metal Anode and Rechargeable Li Metal Batteries*, Springer International Publishing, Switzerland **2017**; f) P. G. Bruce, S. A. Freunberger, L. J. Hardwick, J. M. Tarascon, *Nat. Mater.* **2012**, *11*, 19; g) K. Liu, A. Pei, H. R. Lee, B. Kong, N. Liu, D. Lin, Y. Liu, C. Liu, P.-c. Hsu, Z. Bao, Y. Cui, *J. Am. Chem. Soc.* **2017**, *139*, 4815; h) Y. Lu, K. Korf, Y. Kambe, Z. Tu, L. A. Archer, *Angew. Chem., Int. Ed.* **2014**, *53*, 488; i) F. Ding, W. Xu, G. L. Graff, J. Zhang, M. L. Sushko, X. Chen, Y. Shao, M. H. Engelhard, Z. Nie, J. Xiao, X. Liu, P. V. Sushko, J. Liu, J.-G. Zhang, *J. Am. Chem. Soc.* **2013**, *135*, 4450; j) J. Zheng, M. H. Engelhard, D. Mei, S. Jiao, B. J. Polzin, J.-G. Zhang, W. Xu, *Nat. Energy* **2017**, *2*, 17012; k) D. Lin, Y. Liu, Z. Liang, H.-W. Lee, J. Sun, H. Wang, K. Yan, J. Xie, Y. Cui, *Nat. Nanotechnol.* **2016**, *11*, 626; l) Y.-K. Sun, S.-T. Myung, B.-C. Park, J. Prakash, I. Belharouak, K. Amine, *Nat. Mater.* **2009**, *8*, 320; m) X.-B. Cheng, R. Zhang, C.-Z. Zhao, Q. Zhang, *Chem. Rev.* **2017**, *117*, 10403.

[3] a) D. Aurbach, E. Zinigrad, Y. Cohen, H. Teller, *Solid State Ionics* **2002**, *148*, 405; b) U. von Sacken, E. Nodwell, A. Sundher, J. R. Dahn, *J. Power Sources* **1995**, *54*, 240.

[4] K. Xu, *Chem. Rev.* **2014**, *114*, 11503.

[5] F. Ding, W. Xu, X. Chen, J. Zhang, M. H. Engelhard, Y. Zhang, B. R. Johnson, J. V. Crum, T. A. Blake, X. Liu, J.-G. Zhang, *J. Electrochem. Soc.* **2013**, *160*, A1894.

[6] a) J. Zheng, J. A. Lochala, A. Kwok, Z. D. Deng, J. Xiao, *Adv. Sci.* **2017**, *4*, 1700032; b) S.-K. Jeong, H.-Y. Seo, D.-H. Kim, H.-K. Han, J.-G. Kim, Y. B. Lee, Y. Iriyama, T. Abe, Z. Ogumi, *Electrochem. Commun.* **2008**, *10*, 635; c) Y. Yamada, K. Furukawa, K. Sodeyama, K. Kikuchi, M. Yaegashi, Y. Tateyama, A. Yamada, *J. Am. Chem. Soc.* **2014**, *136*, 5039; d) Y. Yamada, A. Yamada, *J. Electrochem. Soc.* **2015**, *162*, A2406; e) L. Suo, Y.-S. Hu, H. Li, M. Armand, L. Chen, *Nat. Commun.* **2013**, *4*, 1481; f) B. Liu, W. Xu, P. Yan, S. T. Kim, M. H. Engelhard, X. Sun, D. Mei, J. Cho, C.-M. Wang, J.-G. Zhang, *Adv. Energy Mater.* **2017**, *7*, 1602605; g) L. Suo, O. Borodin, T. Gao, M. Olguin, J. Ho, X. Fan, C. Luo, C. Wang, K. Xu, *Science* **2015**, *350*, 938; h) J. Qian, W. A. Henderson, W. Xu, P. Bhattacharya, M. Engelhard, O. Borodin, J.-G. Zhang, *Nat. Commun.* **2015**, *6*, 6362; i) J. Qian, B. D. Adams, J. Zheng, W. Xu, W. A. Henderson, J. Wang, M. E. Bowden, S. Xu, J. Hu, J.-G. Zhang, *Adv. Funct. Mater.* **2016**, *26*, 7094; j) J. Wang, Y. Yamada, K. Sodeyama, C. H. Chiang, Y. Tateyama, A. Yamada, *Nat. Commun.* **2016**, *7*, 12032.

[7] a) H. Wang, M. Matsui, H. Kuwata, H. Sonoki, Y. Matsuda, X. Shang, Y. Takeda, O. Yamamoto, N. Imanishi, *Nat. Commun.* **2017**, *8*, 15106; b) H. Moon, T. Mandai, R. Tatara, K. Ueno, A. Yamazaki, K. Yoshida, S. Seki, K. Dokko, M. Watanabe, *J. Phys. Chem. C* **2015**, *119*, 3957; c) K. Ueno, J. Murai, H. Moon, K. Dokko, M. Watanabe, *J. Electrochem. Soc.* **2017**, *164*, A6088; d) K. Dokko, N. Tachikawa, K. Yamauchi, M. Tsuchiya, A. Yamazaki, E. Takashima, J.-W. Park, K. Ueno, S. Seki, N. Serizawa, M. Watanabe, *J. Electrochem. Soc.* **2013**, *160*, A1304; e) K. Ueno, J. Murai, K. Ikeda, S. Tsuzuki, M. Tsuchiya, R. Tatara, T. Mandai, Y. Umebayashi, K. Dokko, M. Watanabe, *J. Phys. Chem. C* **2016**, *120*, 15792; f) T. Doi, Y. Shimizu, M. Hashinokuchi, M. Inaba, *J. Electrochem. Soc.* **2017**, *164*, A6412.

[8] B. D. Adams, J. Zheng, X. Ren, W. Xu, J.-G. Zhang, *Adv. Energy Mater.* **2018**, *8*, 1702097.

[9] P. S. Pregosin, P. G. A. Kumar, I. Fernández, *Chem. Rev.* **2005**, *105*, 2977.

[10] a) G. Kresse, J. Furthmuller, *Phys. Rev. B* **1996**, *54*, 11169; b) G. Kresse, J. Hafner, *Phys. Rev. B* **1993**, *47*, 558; c) G. Kresse, J. Hafner, *Phys. Rev. B* **1994**, *49*, 14251.

